Journal of Molecular and Cellular Cardiology 129 (2019) 58–68

Contents lists available at ScienceDirect

Journal of Molecular and Cellular Cardiology

journal homepage: www.elsevier.com/locate/yjmcc

Role of the PRC2-Six1-miR-25 signaling axis in heart failure

Jae Gyun Oh[a], Seung Pil Jang[b], Jimeen Yoo[a], Min-Ah Lee[b], Seung Hee Lee[b], Taejoong Lim[b], Eden Jeong[b], Changwon Kho[a], Hyun Kook[c], Roger J. Hajjar[a], Woo Jin Park[b,*], Dongtak Jeong[a,**]

[a] Cardiovascular Research Center, Icahn School of Medicine at Mount Sinai, New York, NY, USA
[b] School of Life Sciences, Gwangju Institute of Science and Technology, Gwangju, South Korea
[c] Basic Research Laboratory, Chonnam National University Medical School, Hwasun-gun, Jeollanam-do, South Korea

ARTICLE INFO

Keywords:
Heart failure
SERCA2a
miRNA-25
Six1
PRC2
Epigenetics

ABSTRACT

The reduced expression of cardiac sarco-endoplasmic reticulum Ca^{2+} ATPase (SERCA2a) is a hallmark of heart failure. We previously showed that miR-25 is a crucial transcriptional regulator of SERCA2a in the heart. However, the precise mechanism of cardiac miR-25 regulation is largely unknown. Literatures suggested that miR-25 is regulated by the transcriptional co-factor, sine oculis homeobox homolog 1 (Six1), which in turn is epigenetically regulated by polycomb repressive complex 2 (PRC 2) in cardiac progenitor cells. Therefore, we aimed to investigate whether Six1 and PRC2 are indeed involved in the regulation of the miR-25 level in the setting of heart failure. Six1 was up-regulated in the failing hearts of humans and mice. Overexpression of Six1 led to adverse cardiac remodeling, whereas knock-down of Six1 attenuated pressure overload-induced cardiac dysfunction. The adverse effects of Six1 were ameliorated by knock-down of miR-25. The epigenetic repression on the *Six1* promoter by PRC2 was significantly reduced in failing hearts. Epigenetic repression of Six1 is relieved through a reduction of PRC2 activity in heart failure. Six1 up-regulates miR-25, which is followed by reduction of cardiac SERCA2a expression. Collectively, these data showed that the PRC2-Six1-miR-25 signaling axis is involved in heart failure. Our finding introduces new insight into potential treatments of heart failure.

1. Introduction

Heart failure (HF) is a leading cause of mortality and morbidity worldwide [1]. In the US, cardiovascular disease accounts for almost one in every three deaths, making it a primary health concern [1]. Thus, there is an urgent need for therapies that have the potential to reverse the course of HF. The cardiac sarco-endoplasmic reticulum Ca^{2+} ATPase (SERCA2a), also known as ATP2A2, plays a critical role in Ca^{2+} cycling during excitation–contraction coupling in cardiomyocytes (CMs). Impaired Ca^{2+} uptake, resulting from decreased expression and reduced activity of SERCA2a, is a hallmark of HF [2]. Accordingly, modulation of SERCA2a activity and expression has proven effective in improving key parameters of HF [3].

Our group recently showed that miR-25 is up-regulated in hearts obtained from humans and mice with severe HF and that miR-25 down-regulates the SERCA2a level by enhancing degradation of the *SERCA2a* mRNA [4]. Delivery of the antagomiR of miR-25 or Tough decoy prevents the progression of HF in mice that have undergone transverse aortic constriction (TAC) surgery. miR-25 is an endogenous regulator of SERCA2a and provides a valuable therapeutic target for the treatment of HF. The miR-106b-25 cluster, which consists of miR-106b, miR-93, and miR-25, resides in the intron of the *MCM7* gene [5]. Sine oculis homeobox homolog (Six) 1, a transcriptional cofactor, was reported to bind the *MCM7* promoter and regulate the expression of the miR-106b-25 cluster in human breast cancer cells [6]. Since miR-25 expression is driven by the *MCM7* promoter, we hypothesized that Six1 might also play a role in HF via up-regulation of miR-25.

Six1 functions normally in early cardiac progenitor cells, but is epigenetically silenced by polycomb repressive complex (PRC) 2 in differentiated cardiac progenitor cells [7]. De-repression of Six1 in embryonic progenitor cells is a precursor for HF. However, the role of Six1 and its epigenetic regulation in adult hearts appear to be unlikely [7]. In contrast, we show in this study that Six1 level is significantly elevated in the adult failing hearts which is due to the relief of PRC2-mediated epigenetic repression. We provide compelling lines of evidence supporting that the PRC2-Six1-miR-25 signaling pathway is implicated in the progress of HF in humans and mice.

* Correspondence to: W. J. Park, College of Life Sciences, Gwangju Institute of Science and Technology (GIST), 123 Cheomdangwagi-ro, Buk-gu, Gwangju 61005, South Korea.
** Correspondence to: D. Jeong, Cardiovascular Research Center, Icahn School of Medicine at Mount Sinai (ISMMS), 1 Gustave L. Levy place, NY, New York, USA.
E-mail addresses: woojinpark@icloud.com (W.J. Park), dongtak.jeong@mssm.edu (D. Jeong).

https://doi.org/10.1016/j.yjmcc.2019.01.017
Received 10 September 2018; Received in revised form 25 December 2018; Accepted 21 January 2019
Available online 13 February 2019

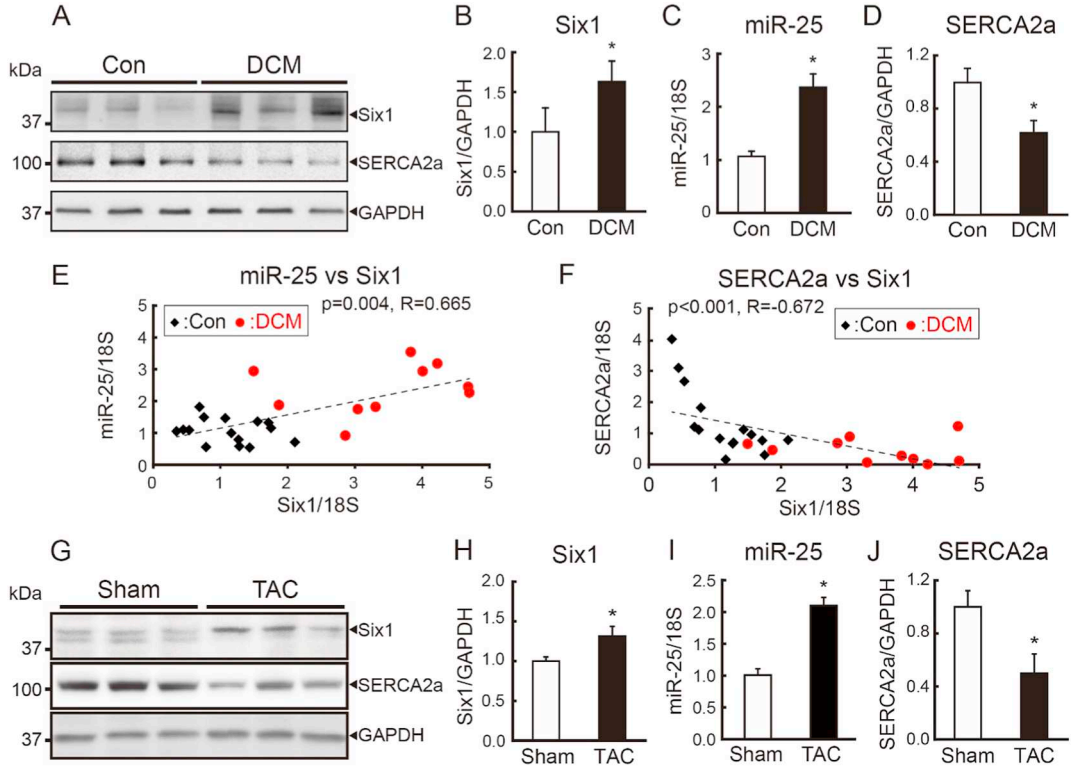

Fig. 1. Six1 is up-regulated in failing hearts.
Representative blot (A) and quantitative analyses showing levels of Six1 (B) and SERCA2a (D) in heart tissue samples obtained from patients with dilated cardiomyopathy (DCM) and from healthy controls (Con). (C) Levels of miR-25 measured by qRT-PCR. Scatter plots showing the relation between *Six1* mRNA and miR-25 levels (E), and between *Six1* mRNA and *SERCA2a* mRNA levels (F) (n = 10–15). Representative blot (G) and quantitative analyses showing levels of Six1 (H) and SERCA2a (I) in heart tissue samples obtained from mice with TAC-induced HF (TAC) and sham-operated mice (Sham). (J) Levels of miR-25 measured by qRT-PCR (n = 6). *, $p < .05$, versus the respective control, as determined by Student's t-test. Data are presented as mean ± s.e.m.

2. Results

2.1. Six1 is up-regulated in failing hearts

To examine the role of Six1 in HF, we first determined Six1 levels in human failing hearts. Western blotting showed that Six1 levels were significantly higher in the hearts of patients with dilated cardiomyopathy (DCM) than in the hearts of normal donors (Con) (Fig. 1A, B). Consistent with our previous reports, the miR-25 level was significantly higher (Fig. 1C) whereas the SERCA2a level was significantly lower in DCM hearts (Fig. 1D). Comparative plotting revealed a significant positive correlation between the transcription levels of miR-25 and Six1 (Fig. 1E; $p = .004$, $R = 0.665$) and a significant negative correlation between the transcription levels of SERCA2a and Six1 (Fig. 1F; $p = .0003$, $R = -0.672$). HF was induced in mice by applying TAC for 6 weeks. Western blotting revealed that the Six1 levels were significantly higher in failing hearts than in normal hearts (Sham) (Fig. 1G, H). miR-25 levels were significantly higher (Fig. 1I), whereas SERCA2a levels were significantly lower, in failing hearts (Fig. 1J). In summary, Six1 is up-regulated in human and mouse failing hearts, and this up-regulation coincides with the up-regulation of miR-25 and the down-regulation of SERCA2a, implying a potential role of Six1 in HF.

2.2. Overexpression of Six1 leads to adverse cardiac remodeling

To further examine the role of Six1 in the heart, we generated transgenic (Tg) mice in which Six1 was overexpressed specifically in the heart under the control of an α-myosin heavy chain (α-MHC) promoter. Overexpression of Six1 was accompanied by the up-regulation of miR-25 and the down-regulation of SERCA2a in the heart (Fig. 2A). The Six1 Tg mice exhibited significantly larger hearts than their non-transgenic littermates (NL) when analyzed 8 weeks after birth (Fig. 2B and C). Measurement of the cross-sectional areas (CSAs) of CMs revealed that Six1 overexpression resulted in hypertrophic remodeling of CMs (Fig. 2B and D). Trichrome staining of the same tissue sections also showed that the hypertrophic remodeling was accompanied by profound fibrosis (Fig. 2B and E). qRT-PCR measurements of the expression levels of the hypertrophic markers, βMHC, atrial natriuretic factor (ANF), and brain natriuretic peptide (BNP), and the fibrotic markers, transforming growth factor-β1 (TGF-β1) and collagen I, further confirmed that Six1 Tg mice exhibited adverse cardiac remodeling characterized by hypertrophy and fibrosis (Fig. 2F).

Echocardiography revealed that the hearts of Six1 Tg mice underwent severe left ventricular (LV) dilations as shown by increased LV internal dimensions at diastole (LVIDd) and systole (LVIDs) with markedly reduced fractional shortening (FS) (Fig. 2G). Contractile properties of isolated CMs were further evaluated with a dual-excitation photomultiplier system. Peak shortening and the rates of contraction and relaxation were significantly impaired in CMs isolated from the Six Tg mice. Furthermore, the amplitudes of Ca^{2+} transients were severely impaired (Fig. 2H). These cardiac defects were associated with high mortality rates of the Six1 Tg mice (Fig. 2I; $p = .0014$). In fact, none of the Six1 Tg mice survived for > 6 months. We initially obtained but failed to maintain two additional Tg lines due to premature sudden deaths. Those Tg lines had higher Six1 protein levels (5–10 times higher than those of non-Tg) and exhibited fatal cardiac remodeling (data not shown). These data suggest that elevated Six1 levels lead to adverse cardiac remodeling and dysfunction.

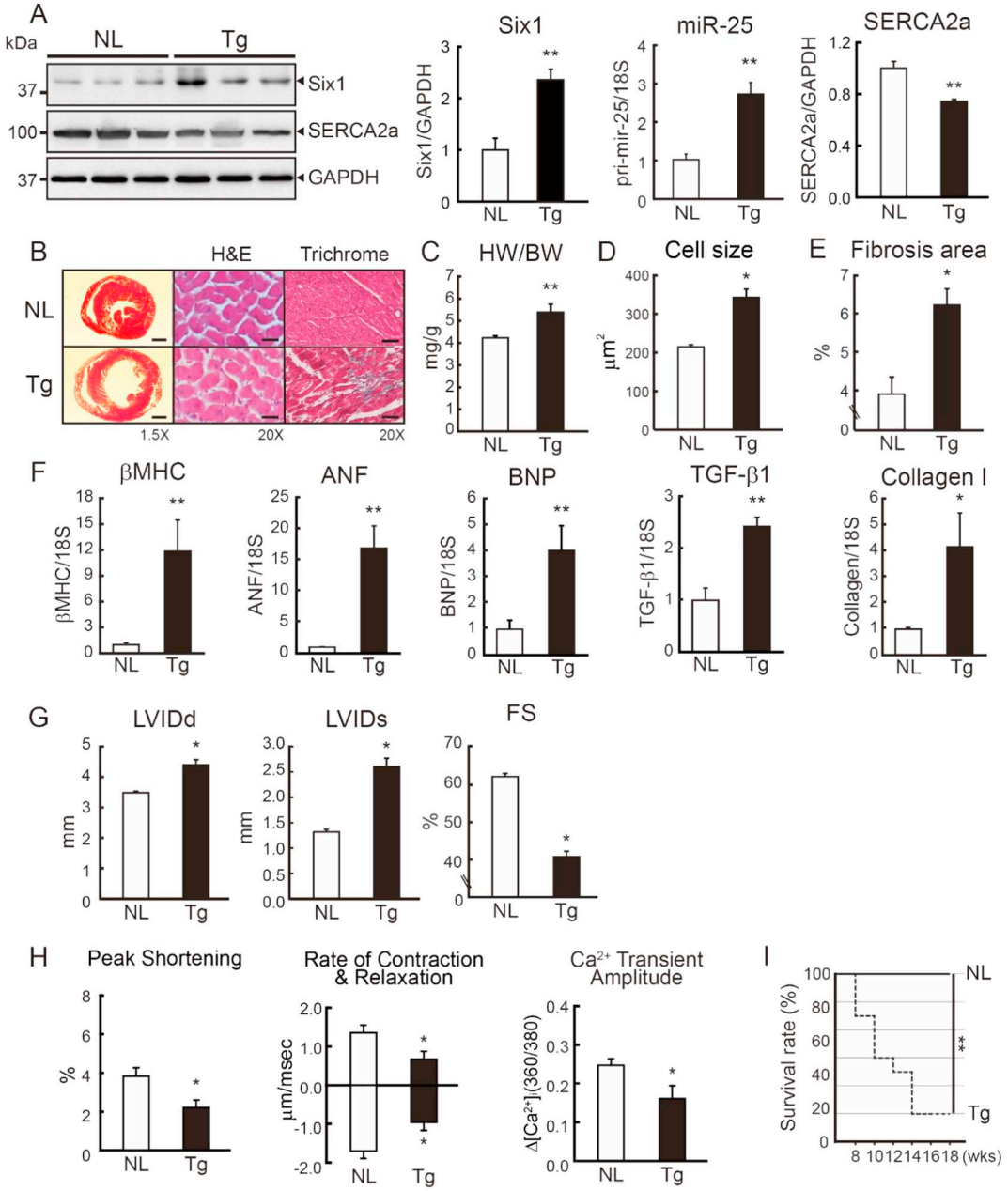

Fig. 2. Overexpression of Six1 leads to adverse cardiac remodeling.
(A) Representative blot and quantitative analyses showing levels of Six1, miR-25, and SERCA2a expression in heart tissue samples obtained from Six1-overexpressing transgenic mice (Tg) and the negative littermates (NL). (B) Representative images of a mouse heart cross-section, H&E stain, and Masson's trichrome stain. Scale bars, 1 mm, 20 μm, and 20 μm, respectively. (C) Quantifications of heart weight/body weight ratio. (D) Means of cardiomyocyte cross-sectional area (CSA) (n = 150–200 cells/4 hearts). (E) Percentages of fibrotic areas. (F) Quantitative analyses of hypertrophic markers (βMHC, ANF, BNP) and fibrotic markers (TGF-β1, Collagen I). (G) Echocardiographic parameters. LVIDd, left ventricular internal dimension-diastole; LVIDs, left ventricular internal dimension-systole; FS, fractional shortening. (H) Averaged data of peak shortening, rate of contraction and relaxation, and Ca^{2+} transient amplitude (n = 100–150 cells/4 hearts). (I) Survival rate of Six1 Tg and NL. The Kaplan–Meier method was used to analyze animal lifespan (n = 28–30). *, $p < .05$, versus the NL control, as determined by Student's t-test. Data are presented as mean ± s.e.m.

2.3. Knock-down of Six1 ameliorates pressure overload-induced cardiac remodeling

To further understand the role of Six1 in HF, we utilized adeno-associated virus serotype 9 (AAV9) expressing a short interfering RNA of Six1, AAV9 siSix1. HF was induced in mice by applying TAC for 8 weeks, and then AAV9 siSix1 or control virus, AAV9 Cont, was injected via the tail vein. Molecular and functional analyses were performed 4 weeks post-injection (Fig. 3A). As shown in Fig. 1, Six1 levels were elevated in the heart upon TAC. However, the induced Six1 levels were significantly normalized by AAV9 siSix1 (Fig. 3B and C). In parallel, miR-25 and SERCA2a levels were also normalized (Fig. 3B and C). Cardiac hypertrophy and fibrosis were significantly blunted by AAV9 siSix1 as shown by normalized heart weights (Fig. 3D and E), CSA of CMs (Fig. 3F), and Picro Sirus Red-stained fibrotic areas (Fig. 3G). These observations were further confirmed by normalization of expression levels of hypertrophic and fibrotic markers as determined by qRT-PCR (Fig. 3H). FS was prominently reduced upon TAC and further deteriorated during the additional 4 weeks following the injection of control AAV9. However, this deterioration of cardiac function was

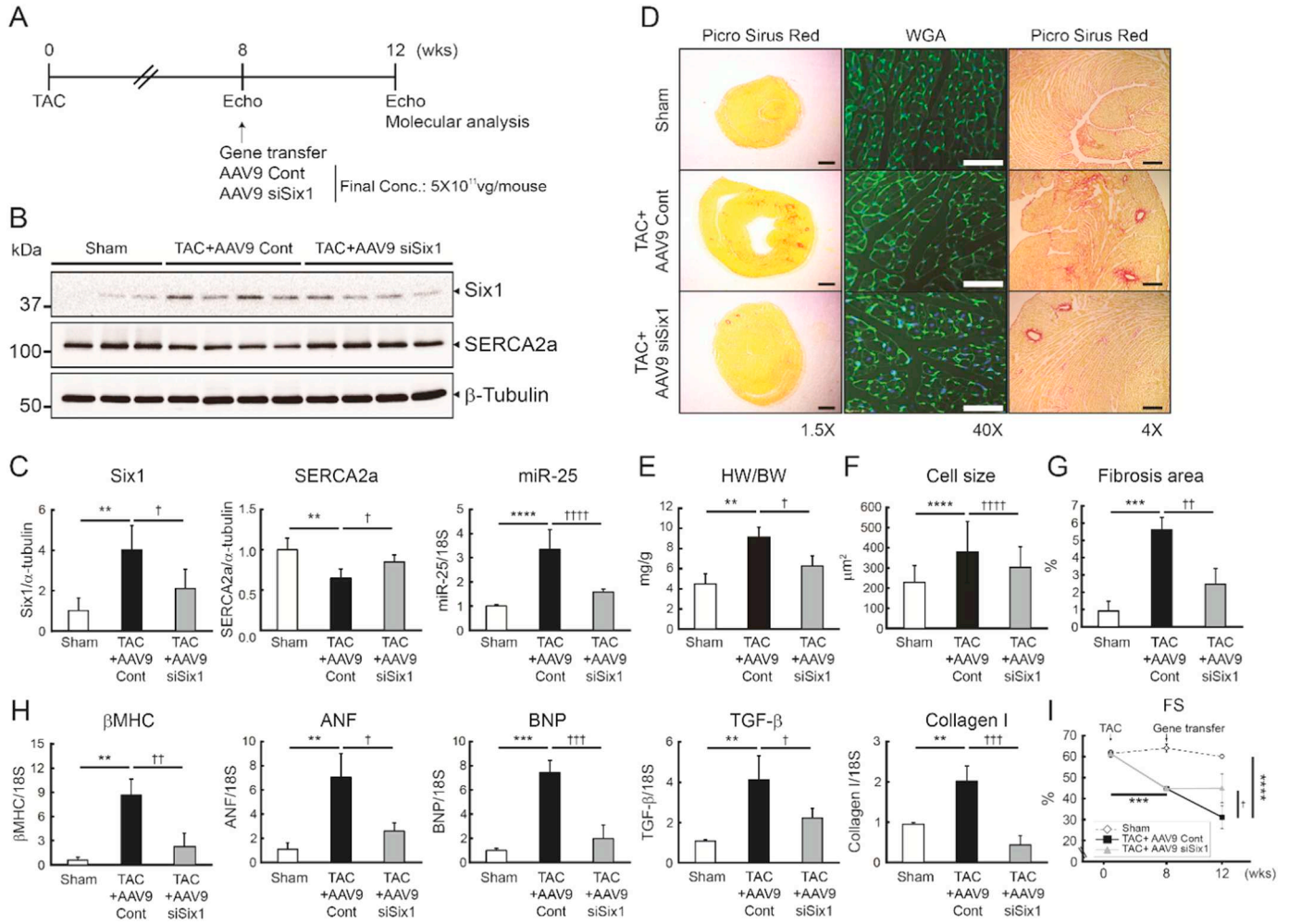

Fig. 3. Knock-down of Six1 ameliorates pressure overload-induced cardiac remodeling.
(A) Experimental schema for AAV9 siSix1 gene transfer in a mouse model of HF. Six-week-old male B6C3/F1 mice were subjected to TAC and received AAV9 carrying siSix1 (AAV9 siSix1, 5×10^{11} vg/mouse) or scrambled siRNA (AAV9 Cont) via tail-vein injection 8 weeks post-TAC surgery. Cardiac function was measured by echocardiography, and molecular changes were analyzed by Western blotting and qRT-PCR 4 weeks after gene delivery. Representative blot (B) and quantitative analyses (C) showing levels of Six1, miR-25, and SERCA2a expression. (D) Representative images of a mouse heart cross-section, WGA stain, and Picro Sirus Red stain. Scale bars, 1 mm, 20 μm, and 100 μm, respectively. (E) Quantifications of heart weight/body weight ratio. (F) Means of cardiomyocyte cross-sectional area (CSA) (n = 150–200 cells/4 hearts). (G) Percentages of fibrotic areas. (H) Quantitative analyses of hypertrophic markers (βMHC, ANF, BNP) and fibrotic markers (TGF-β1, Collagen I). (I) Fractional shortening (FS) (n = 6). *, $p < .05$, **, $p < .01$, ***, $p < .001$ versus sham-operated mice and †, $p < .05$, ††, $p < .01$, †††, $p < .001$ versus the TAC-operated mice infected with AAV9 Cont, as determined by one-way ANOVA Bonferroni test. Data are represented as mean ± s.e.m. in all panels. (For interpretation of the references to colour in this figure legend, the reader is referred to the web version of this article.)

prevented by AAV9 siSix1 (Fig. 3I). Collectively, the data obtained from the gain-of-function (Fig. 2) and the loss-of-function (Fig. 3) approaches indicate that Six1 plays a critical role in HF, probably through up-regulation of miR-25, in mice.

2.4. Six1 directly elevates the miR-25 level

There are three putative Six1 binding sites, E2F domains 1–3, in the *MCM7* promoter. We generated luciferase reporter plasmids containing the full length *MCM7* promoter and ones with various deletions; E2F domain 1 deletion mutant (ΔI), E2F domain 2 deletion mutant (ΔII), E2F domain 3 deletion mutant (ΔIII), and dE2F domain 1–3 deletion mutant (ΔI-III) (Fig. 4A). Each plasmid was transfected into H9c2 cells alone or in combination with a Six1 expression plasmid. Transcriptional activity of the full length *MCM7* promoter was remarkably enhanced by Six1 in a dose-dependent manner. However, the MCM7 promoters with the E2F domain deletions, except ΔIII, exhibited significantly reduced transcriptional activity (Fig. 4B). This indicates that the E2F domains 1 and 2 are essential for the binding of Six1 to the *MCM7* promoter. Chromatin immunoprecipitation was performed using a primer pair indicated with arrows in Fig. 4A to see if Six1 binds to the *MCM7* promoter in vivo. The results indicate that Six1 binds to the *MCM7* promoter in the mouse hearts. Intriguingly, this interaction was more prominent under pathological conditions (Fig. 4C). A recombinant adenovirus that expresses Six1, Ad Six1, was generated. Ad Six1-mediated overexpression of Six1 resulted in the up-regulation of miR-25 and down-regulation of SERCA2a in isolated CMs using western blot and qRT-PCR experiments (Fig. 4D and E, respectively). Two other members of the miR-106b-25 cluster, miR-106b and miR-93, were also up-regulated by the overexpression of Six1 (Fig. 4F). These data suggest that Six1 directly regulates the expression of miR-25 via binding to the *MCM7* promoter in CMs. CMs transfected with Ad Six1 exhibited reduced contractility as shown by the reduced peak shortening, the rates of relaxation and contraction, and the reduced Ca^{2+} transient amplitude (Fig. 4G). Taken together, these data suggest that Six1 reduces contractility of CMs through miR-25-mediated down-regulation of SERCA2a.

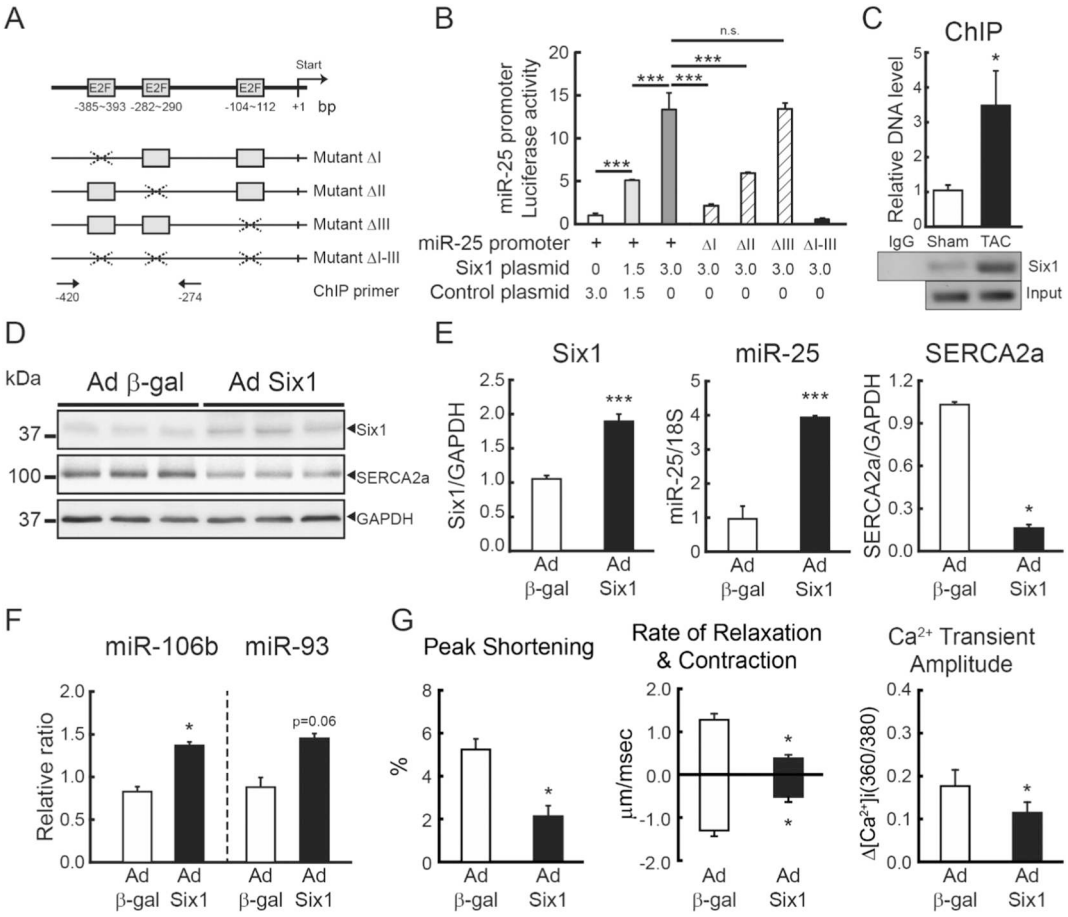

Fig. 4. Six1 elevates the miR-25 level.

(A) Schematic representation of the *MCM7* (miR-25) promoter region. The E2F sites are framed by boxes. Deletion mutant constructs (Mutant ΔI, II, III and I-III) for entire luciferase assay are illustrated. Deleted E2F domain is indicated with X. Arrows indicate a primer pair used for PCR in ChIP assays. Numbers represents the starting position of each primer from the translation initiation codon (+1). (B) Luciferase reporter assay. Luciferase reporter with a *MCM7* promoter or mutant (0.25 μg) was co-transfected into H9c2 cells with Six1 plasmid or empty plasmid (control) for 24 h, and luciferase activity was determined ($n = 4$). (C) Chromatin immunoprecipitation (ChIP) assay. Normal (sham) or failing hearts (6 weeks post-TAC; TAC) were analyzed ($n = 5$). The assay was performed with anti-Six1 antibody or control IgG. A pair of primers specific for −420 to −274 region containing E2F sites was used in qRT-PCR. The input represented the DNA in crude tissue extract before the immunoprecipitation. Representative western blot (D) and quantitative analyses (E) showing levels of Six1, miR-25, and SERCA2a expression in isolated adult mouse cardiomyocytes that were infected with an adenovirus encoding Six1 (Ad Six1) or β-galactosidase (Ad β-gal, control) for 48 h. (F) Quantitative analyses of other members of the miR-106b-25 cluster. (G) Averaged data of peak shortening, rate of contraction and relaxation, and Ca^{2+} transient amplitude ($n = 100$–150 cells/4 hearts). *, $p < .05$, ***, $p < .001$ versus the Ad β-gal control, as determined by Student's *t*-test. Data are presented as mean ± s.e.m.

2.5. Six1 leads to adverse cardiac remodeling through miR-25

Six1 might regulate other target genes in addition to the miR-106b-25 cluster. Thus we evaluated the significance of the Six1-miR-25 signaling axis during HF using an AAV9 that expresses Six1, AAV9 Six1, and another AAV9 that expresses a tough decoy (TuD) of miR-25, AAV9 TuD [8]. AAV9 Six1 alone or AAV9 Six1 and AAV9 TuD were injected into mice via the tail vein, and the consequences were evaluated at 4 weeks post-injection (Fig. 5A). Injection of AAV9 Six1 up-regulated the levels of Six1 and miR-25 and down-regulated the level of SERCA2a as observed in Six1 Tg mice. However, co-injection with AAV9 TuD normalized the altered levels of miR-25 and SERCA2a without affecting the level of Six1 (Fig. 5B and C). The AAV9 Six1-mediated increases in heart weight and fibrosis were significantly normalized by AAV9 TuD (Fig. 5D, E and G). No significant changes were observed in CSA (Fig. 5F), it may be because a longer time is needed for discernible effects on cell size. The AAV9 Six1-mediated up-regulation of hypertrophic and fibrotic markers was also normalized by AAV9 TuD (Fig. 5H). While Six1 reduced cardiac function as shown by the profoundly reduced FS, this detrimental consequence was significantly ameliorated by AAV9 TuD (Fig. 5I). These data indicate that the up-regulation of miR-25 significantly, albeit not entirely, contributes to the Six1-mediated adverse cardiac remodeling.

2.6. Six1 is epigenetically regulated in failing hearts

A previous study reported that the expression of Six1 remains repressed by PRC2 in postnatal and adult hearts [7]. To determine if epigenetic regulation is involved in increased Six1 expression during HF, we first examined the expression levels of PRC2 components in failing hearts obtained from human patients. Western blotting revealed that the level of EED, a critical regulator of PRC2 activity, was remarkably lower in the hearts of DCM patients, while the levels of other components, SUZ12 and EZH2, were not significantly altered (Fig. 6A). qRT-PCR also showed that *EED* mRNA levels were significantly lower in DCM patients (Fig. 6B). Correlation analysis revealed that there was a significant negative correlation between the transcription levels of EED and Six1 (Fig. 6C, left panel; $p < .0001$, $R = -0.722$), and a significant positive correlation between the transcription levels of EED and SERCA2a (Fig. 6C, right panel; $p = .003$, $R = 0.802$). All three components of PRC2 were significantly reduced in the failing hearts of mice subjected to TAC for 8 weeks (Fig. 6D). To further determine if

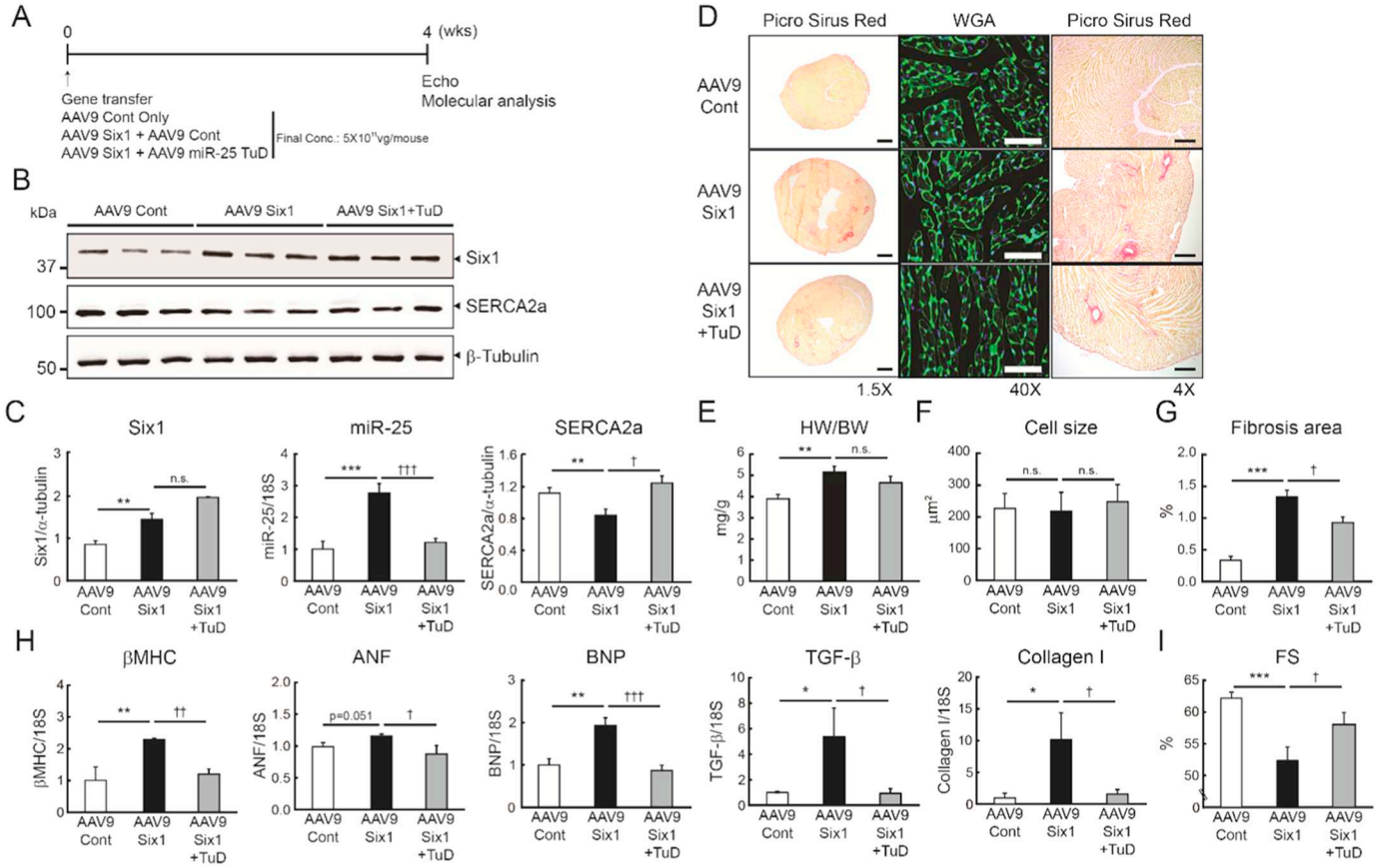

Fig. 5. Six1 leads to adverse cardiac remodeling through miR-25.
(A) Experimental schema for Six1 and a tough decoy RNA of miR-25 (TuD) gene transfer to test the Six1-miR-25 axis. Six-week-old male B6C3/F1 mice received AAV9 Six1 alone or AAV9 Six1 and AAV9 TuD simultaneously via the tail vein (AAV9 Six1, 5×10^{11} vg/mouse; AAV9 TuD, 5×10^{11} vg/mouse). Cardiac function was measured by echocardiography, and molecular changes were analyzed by Western blotting and qRT-PCR 4 weeks after gene delivery. Representative blot (B) and quantitative analyses (C) showing levels of Six1, miR-25, and SERCA2a expression. (D) Representative images of a mouse heart cross-section, WGA stain, and Picro Sirus Red stain. Scale bars, 1 mm, 20 μm, and 100 μm, respectively. (E) Quantifications of heart weight/body weight ratio. (F) Means of cardiomyocyte cross-sectional area (CSA) (n = 150–200 cells/4 hearts). (G) Percentages of fibrotic areas. (H) Quantitative analyses of hypertrophic markers (βMHC, ANF, BNP) and fibrotic markers (TGF-β1, Collagen I). (I) Fractional shortening (FS) (n = 5). *, $p < .05$, **, $p < .01$, ***, $p < .001$ versus the mice infected with AAV9 Cont and †, $p < .05$, ††, $p < .01$, †††, $p < .001$ versus the mice infected with AAV9 Six1, as determined by one-way ANOVA Bonferroni test. Data are represented as mean ± s.e.m. in all panels. (For interpretation of the references to colour in this figure legend, the reader is referred to the web version of this article.)

epigenetic regulation of Six1 was indeed involved during HF, we examined the levels of histone modifications, DNA methylation, and occupancy of transcription machinery in the promoter region of *Six1* by chromatin immuno-precipitation. The trimethylation of histone H3 at lysine 27 (H3K27me3) and binding of SUZ12 in the Six1 promoter were significantly reduced in the failing hearts (Fig. 6E). Furthermore, acetylation of histone H3 (AcH3) and binding of RNA polymerase II (Pol II) were enhanced in the failing hearts (Fig. 6E). Collectively, these data suggest that the repression of the *Six1* promoter by PRC2 was significantly relieved. Lastly, bisulfite sequencing revealed that DNA methylation at CpG islands in the promoter region of Six1 was significantly reduced (Fig. 6F). Notably, prominent unmethylation was observed at the three CpG islands located 200, 116, and 40 bp upstream of the transcription start site during HF.

In summary, we propose a signaling pathway whereby cardiac stress impairs PRC2-mediated repression of Six1, thus leading to enhanced expression of Six1. One of the critical targets of Six1 is miR-25, which reduces the SERCA2a level. This reduction is, in turn, responsible for the contractile dysfunction in HF (Fig. 6G). This signaling axis therefore provides a valuable target for the development of therapeutic modalities for HF.

3. Discussion

HF remains a major cause of morbidity and mortality. Research has uncovered novel therapeutic options through investigation of intracellular and molecular mechanisms. One profound feature of HF is the reduced expression and activity of SERCA2a, which results in impaired Ca^{2+} regulation in the heart [2]. Restoration of SERCA2a by gene transfer was shown to improve cardiac function in failing hearts using various preclinical and clinical approaches [3,9–16]. Therefore, the manipulation of the expression and activity of SERCA2a has been considered a valuable modality for the treatment of HF [8,17–21]. One such modality is the inhibition of a microRNA, miR-25, which is up-regulated in failing hearts and directly reduces SERCA2a expression [4]. While AAV-mediated overexpression of miR-25 resulted in cardiac dysfunction, antisense oligonucleotide-mediated down-regulation of miR-25 markedly halted established HF in mice [4]. We further showed that a single injection of a more stable inhibitor of microRNA, TuD, against miR-25 is highly effective in ameliorating cardiac dysfunction, especially through reduction of cardiac fibrosis in the failing heart [8].

In this study, we aimed to elucidate upstream signaling pathways that regulate the expression of miR-25 in the failing heart. It was previously shown that the miR-106b-25 cluster is regulated by Six1, an important mediator of breast cancer progression and metastasis [6].

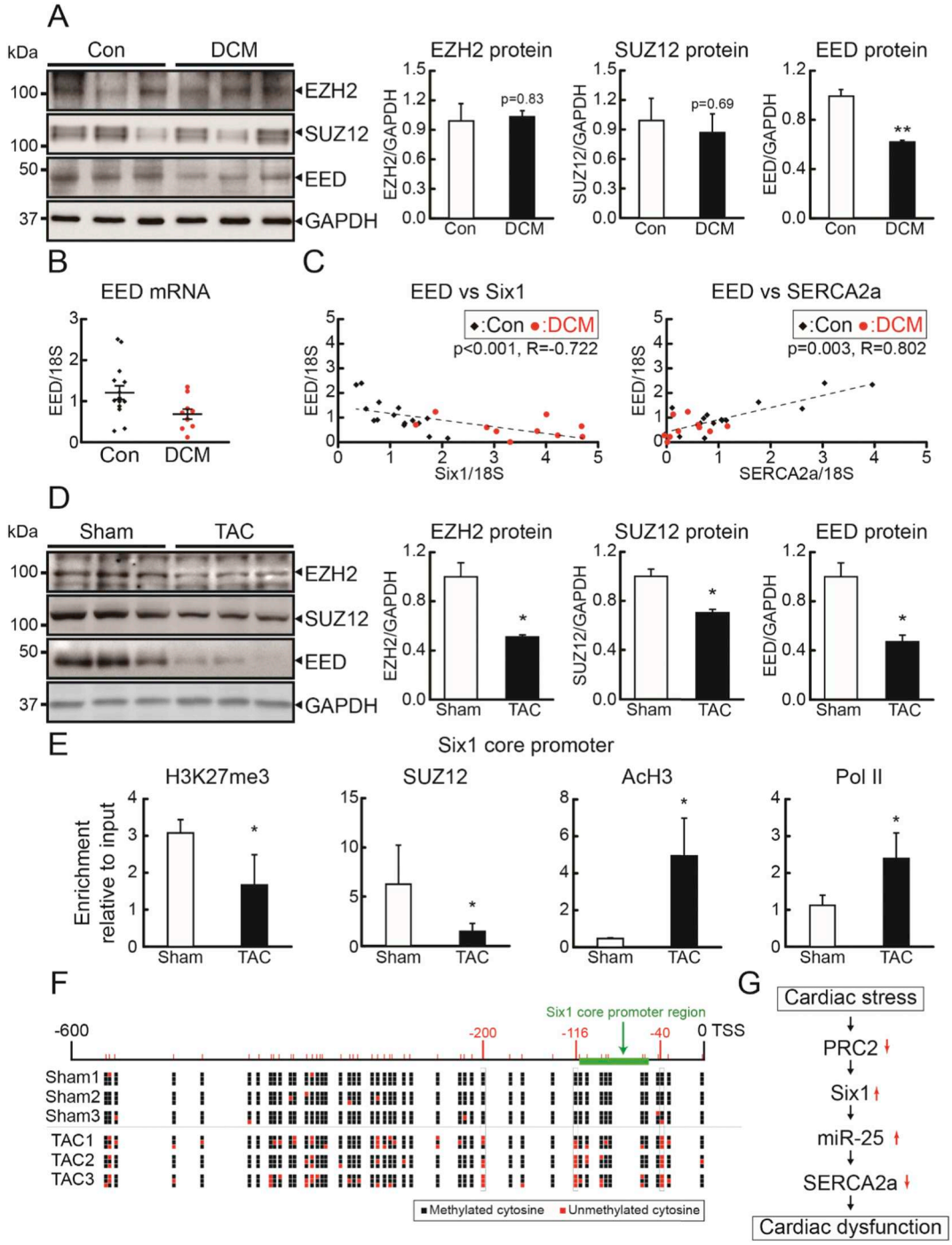

Fig. 6. Six1 is epigenetically regulated in failing hearts.
(A) Representative blot and quantitative analyses showing levels of the polycomb repressor complex 2 (PRC2) components, EZH2, SUZ12, and EED, in heart tissue samples obtained from patients with dilated cardiomyopathy (DCM) and from healthy controls (Con). Levels of *EED* mRNA measured by qRT-PCR (B). Scatter plots showing the relation between *EED* and *Six1* mRNA levels, and between *EED* and *SERCA2a* mRNA levels (C) (n = 10–15). (D) Representative blot and quantitative analyses showing levels of the polycomb repressor complex 2 (PRC2) components, EZH2, SUZ12, and EED, in heart tissue samples obtained from mice with TAC-induced HF (TAC) and sham-operated mice (Sham). (E) Chromatin immunoprecipitation for trimethylation of histone H3 at lysine 27 (H3K27me3), SUZ12, acetylation of histone H3 (AcH3), and RNA polymerase II (Pol II) on the *Six1* core promoter in hearts from TAC or Sham mice. (F) Methylation status of the *Six1* core promoter determined by bisulfite sequencing (n = 3). (G) Schematic representation of the proposed signaling pathway. *, $p < .05$, versus the respective control, as determined by Student's *t*-test. Data are presented as mean ± s.e.m.

Six1 is a homolog of the Drosophila Sine oculis (So) gene that contains a DNA-binding homeodomain and an upstream SIX domain [22]. Six1 recruits Eyes absent (Eya), a transcriptional coactivator and a protein phosphatase, and they synergistically modulate various developmental processes in *Drosophila* [23]. In fact, six isoforms of Six family proteins and four isoforms of Eya family proteins have been identified to cooperate in the regulation of downstream genes [23–33]. Thus, we hypothesized that Six1 is an upstream regulator of miR-25 during HF.

We first evaluated the clinical relevance of Six1 by examining the Six1 levels in normal and DCM human patients. As shown in Fig. 1, Six1

and miR-25 were substantially induced in DCM patients and a significant negative correlation between SERCA2a and Six1 was observed (Fig. 1A–F). Similar molecular profiles were observed in TAC-induced HF mouse models. Six1 Tg exhibited an extremely high mortality: the majority of mice died within 10 weeks with severe cardiac abnormality (Fig. 2). AAV9 Six1-mediated overexpression of Six1 led to a slight increase in apoptosis as assessed by TUNEL assay, although apoptotic markers such as Bim and activated caspase 3 were not significantly induced (Supplementary Fig. S1). These data suggest that Six1 plays an adverse role during HF, thus antagonizing Six1 might be a valuable therapeutic modality for HF. As expected, knock-down of Six1 level with siSix1 significantly ameliorated cardiac dysfunction and fibrosis in mice under pathological conditions (Fig. 3).

The *MCM7* promoter contains three transcription factor binding domains, called E2F. However, a specific binding domain for the regulation of miR-106b-25 cluster has not been identified. Therefore, four different deletion mutants were generated by recombination technique and each construct was evaluated by luciferase reporter activity (Fig. 4). Our results showed that E2F domains 1 and 2 were the major binding motifs for Six1 interaction, but not E2F domain 3. ChIP assay also confirmed the binding of Six1 to the E2F domains 1–2 in vivo and further showed that binding was significantly elevated under pathological conditions. miR-25 TuD, which specifically reduced the level of miR-25, but not those of miR-106b and miR-93 (Supplementary Fig. S2), ameliorated the detrimental effects of Six1 (Fig. 4). Therefore, the roles of miR-106b and miR-93 in HF appear to be minor, although they are localized in the same cluster and up-regulated under cardiac stress conditions.

We further investigated whether Six1 induces HF through up-regulation of miR-25. As shown in Fig. 5, cardiac dysfunction induced by Six1 overexpression was prevented by co-transfer with miR-25 TuD. Our data reaffirmed that Six1-induced HF is indeed induced through up-regulation of miR-25, which in turn down-regulates SERCA2a. Other targets of Six1 may contribute to the progression of HF. However, we reconfirmed other members of the miR-106b-25 cluster, miR-106b and miR-93, have minimal activity in relation to Six1and are not HF-related effector molecules. Taken together, our results suggest that miR-25 is a major mediator of Six1-induced cardiac dysfunction.

We initially found that the Six1-miR-25 axis is associated with HF and then we further tried to identify upstream regulator(s) of Six1 to decipher the entire signaling pathway. Recent literatures have shown that Six1 is epigenetically regulated by the PRC2 complex in embryos [7,34,35]. The epigenetic repression of Six1 in differentiated cardiac progenitor cells is essential for postnatal cardiac homeostasis [7]. However, this study exhibited that it was unlikely that PRC2-mediated epigenetic regulation on Six1 is involved in HF because the expression levels of Six1 and Ezh2, a critical component of PRC2, were not altered in adult mouse hearts that were subjected to TAC [7]. However, their analysis for the epigenetic regulation of PRC2 components was performed within 48 h after TAC, when compensatory hypertrophic responses, but not decompensatory HF responses, occur. Therefore, we evaluated the expression levels of PRC2 components and Six1 in the failing heart 8 weeks after TAC. Six1 was significantly up-regulated in the failing hearts of humans and mice. In parallel, EED, a major component of PRC2 complex, was substantially reduced in the same samples, which suggested that de-repression of Six1 is a fundamental mechanism underlying HF. We found that methylations in the three CpG sites, which are highly conserved across species and considered as putative epigenetic regulation sites in the *Six1* promoter region due to its proximity to the core promoter region, are significantly reduced as shown by our bisulfite sequencing results. Intriguingly, the levels of EZH2 and SUZ12, two other components of PRC2 complex, were not altered in human patients with end-stage HF, while they were significantly down-regulated in HF mice. This result implies that epigenetic alteration on the specific sites of same promoter can be modulated by various contributors in different species.

In summary, our data established a new signaling axis, PRC2-Six1-miR-25, which is shared in the failing hearts across species. Therefore, our data provides new insight into a pathological pathway in HF.

4. Methods

4.1. Human samples

All human tissue samples were obtained from patients under protocols approved by the Institutional Review Board of the Icahn School of Medicine at Mount Sinai. Gene expression was analyzed in human myocardium tissues obtained from patients with DCM ($n = 10$) or from healthy donors ($n = 15$). Tissues were frozen in liquid nitrogen and stored at −80 °C.

4.1.1. Animal care and TAC

All procedures were approved by and performed in accordance with the Institutional Animal Care and Use Committee of the Mount Sinai School of Medicine. The investigation conformed to the Guide for the Care and Use of Laboratory Animals published by the US National Institutes of Health (NIH Publication No. 85–23, revised 1996). Studies were conducted in male C57BL/6 mice aged 8–10 weeks (weight, 25–30 g) obtained from Jackson Laboratories. Mice were anesthetized with a solution mixture of 95 mg/kg ketamine and 5 mg/kg xylazine administered via intraperitoneal injection. Mice were ventilated with a tidal volume of 0.2 mL and a respiratory rate of 110 breaths per minute (Harvard Apparatus). A longitudinal incision of 2–3 mm was made in the proximal sternum to allow visualization of the aortic arch. The transverse aortic arch was ligated between the innominate and left common carotid arteries with an overlaid 27-gauge needle. The needle was then immediately removed, leaving a discrete region of constriction. To evaluate the consistency of the TAC model, pressure gradients, FS, and wall thickness were tested by echocardiography. Then, the qualified animals were randomly allocated to two groups. A < 5% difference in the mean of FS, interventricular septum thickness at end-diastole (IVSd), and body weight was present among the experimental groups. Sham-operated animals underwent the same surgical procedures, except that the ligature was not tied.

4.1.2. Generation of Tg mice

Full-length mouse *Six1* cDNA (NM_009189; OriGene) with the human growth hormone 3′ UTR and a 5.5 kb segment of the α-MHC promoter was constructed and microinjected into FVB fertilized eggs. Integration of the transgene was confirmed by Southern blotting (Macrogen, Korea). Tg mice and negative littermates were analyzed at 8–10 weeks of age.

4.1.3. AAV production and injection

Self-complementary AAV (serotype 9) constructs were generated using the pds-AAV2-EGFP vector and mouse *Six1* gene. The recombinant AAV was produced by transfecting 293 T cells as described previously [25]. The AAV particles in the cell culture media were precipitated with ammonium sulfate and purified by ultracentrifugation on an iodixanol gradient. The particles were then concentrated using a centrifugal concentrator. The AAV titer was determined by qRT-PCR and SDS-PAGE. AAV9 Cont, AAV9 Six1, AAV9 siSix1, or AAV9 miR-25 TuD (5×10^{11} viral genome/mouse) was injected into the tail vein of C57BL/6 mice, and the phenotype of the heart was examined after 4 weeks.

4.1.4. Adenovirus generation and treatment

Adenovirus encoding the *Six1* gene was generated using the pAdEasy XL adenoviral vector system (Stratagene) according to the manufacturer's protocols. Briefly, the entire mouse *Six1* cDNA was subcloned into the *Not*I/*Sal*I site of pShuttle-IRES-hrGFP vector (Stratagene). The isolated cardiomyocytes were infected with Ad β-gal

or Ad Six1 at a MOI of 50 for 48 h.

4.2. Generation of mutant MCM7 promoter

A 2160 bp segment of the human *MCM7* promoter was obtained from human cardiac genomic DNA by PCR using the following primers (forward: 5′-ATT GGT ACC GTG AAG GAT CCT GCG ACA CA-3′, reverse: 5′-ATT AAG CTT GCG TAG TCC TTC AGT GCC AT-3′) [36]. This was subsequently subcloned into the pMCS-Red Firefly Luc vector (Thermo Scientific). Deletion mutagenesis was conducted on the three domain of the human MCM7 promoter within the pMCS-Red Firefly Luc vector. Deletion of each individual domain and a total deletion of all domains were generated using the Q5 Site-Directed Mutagenesis Kit (New England Biolabs). All primers were designed with 5′ ends annealing back-to-back and using the NEB online design software, NEBaseChanger™. The annealing temperatures for all primers were 72 °C. For the deletion of E2F domain 1, the following PCR primers were used: Forward 5′-GCC TGC CCC GCC CTG CGG-3' Reverse 5′-TTG TCT ACT CTC CAG AAC GGC CAT GAT TTC CCA ATT CTT CAT TCT GTC C-3′. For the deletion of E2F domain 2, the following PCR primers were used: Forward 5′-CCT GCA CTA CCC CGC CCG-3′ Reverse 5′-GAG CTG GCG CGG GCG GAG-3′. For the deletion of E2F domain 3, the following PCR primers were used: Forward 5'-TCG GTT GGC CGG CCA CAG-3′ Reverse 5′-CCC CCC ACG TGA CCG GCG-3′. For the deletion of all E2F domains, the following PCR primers were used: Forward 5′-TCG GTT GGC CGG CCA CAG-3′ Reverse 5′- TTG TCT ACT CTC CAG AAC GGC CAT G-3′.

4.3. Luciferase assay

Generated luciferase plasmids were transfected into H9c2 rat cardiomyoblasts with pcDNA vector encoding mouse *Six1* cDNA or empty vector using polyethyleneimine (PEI) transfection reagent. After 24 h, cells were harvested using lysis buffer from the Pierce Firefly Luciferase Glow Assay Kit (Thermo Scientific) and quantified by bovine serum albumin (BSA) assay reagents (Thermo Scientific). Ten micrograms of total lysate was used for each sample, and measurement was performed using a 1450 MicroBeta TriLux Microplate Scintillation and Luminescence Counter (PerkinElmer).

4.4. Ca^{2+} transient and contractility measurement

Cardiomyocytes were isolated from B6C3/F1 mouse hearts by the Langendorff-based method as previously described with minor modifications [27]. In brief, male C57BL/6 mice aged 8–10 weeks were used. An aorta was retrogradely perfused at 37 °C for 3 min with Tyrode buffer (137 mmol/L NaCl, 5.4 mmol/L KCl, 1 mmol/L $MgCl_2$, 10 mmol/L glucose, 10 mmol/L HEPES [pH 7.4], 10 mmol/L 2, 3-butanedione monoxime, and 5 mmol/L taurine) gassed with 100% O_2. The enzymatic digestion was initiated by the addition of collagenase type B (300 U/mL; Worthington) and hyaluronidase (0.1 mg/mL; Worthington) to the perfusion solution. After 20 min of digestion, the left ventricle was removed, cut into several chunks, and gently pipetted for 2 min in Tyrode buffer with 5% BSA. The isolated cardiomyocytes were plated on laminin-coated coverslips and infected with adenoviruses after 2 h of stabilization. The mechanical properties of ventricular myocytes were assessed using a video-based edge detection system (IonOptix). Cardiomyocytes were stimulated to contract at 1 Hz. Changes in sarcomere length were captured and analyzed using soft edge software (IonOptix). To detect intracellular Ca^{2+} changes, cardiomyocytes were loaded with 0.5 μmol/L Fura2-AM (Life Technologies), a Ca^{2+}-sensitive indicator, for 10 min at 37 °C. Fluorescence emissions were recorded by IonOptix simultaneously with contractility measurements.

4.5. Echocardiography

Transthoracic echocardiography was performed using a Vivid 7000 (GE Healthcare) equipped with a H13L transducer (14 MHz). Two-dimensional and M-mode images were obtained in the short-axis view. The heart rate, LV end-diastolic internal diameter, and LV end-systolic internal diameter were measured in at least three repeated cardiac cycles. The ejection fraction and FS were then calculated.

4.6. Histological examination of cardiac tissues

Mouse heart tissues were cryopreserved with optimum cutting temperature compound (Tissue-Tek) and sectioned into 5 μm thick slices. To measure the cell size, a H&E staining kit (9,990,001; Fisher Scientific) was used for staining of the sectioned hearts. Cells are stained pink, and nuclei blue. The CSA was imaged by light microscopy (E400, Nikon) and analyzed using ImageJ software (NIH) at 40× magnification. At least 150 cardiomyocytes were measured per heart. To measure the fibrotic areas, a Masson trichrome staining kit (ab150686; Abcam) was used for staining of the sectioned hearts. The fibrotic area was stained blue, and the normal tissue was stained red. The fibrotic area was calculated as the ratio of the total area of fibrosis to the total area of the section using ImageJ software.

5. Western blot analysis

Membrane and tissue homogenates were prepared as previously described [28]. Proteins were resolved on 10% SDS-PAGE gels followed by transfer to polyvinylidene fluoride membranes (Millipore). Detection of the proteins bands was performed according to standard lab protocols. The membranes were incubated with antibodies against Six1 (ab211359, Abcam, 1:1000), SERCA2a (custom antibody from 21st Century Biochemicals, 1:3000), EZH2 (3147, Cell Signaling, 1:1000), SUZ12 (39,357, Active Motif, 1:1000), EED (PA5–22219, Thermo Fisher Scientific, 1:1000), GAPDH (G8795, Sigma, 1:10,000), and α-tubulin (ab4074, Abcam, 1:10,000).

5.1. Quantitative real-time PCR

Total RNA was isolated with mirVana miRNA Isolation Kit (Ambion). Reverse transcription was performed using qScript microRNA cDNA Synthesis Kit (Quanta). PCR was performed using an ABI PRISM Sequence Detector System 7500 (Applied Biosystems) with SYBR Green (Quanta) as the fluorescent dye and ROX (Quanta) as the passive reference dye. The relative amount of each gene to 18S rRNA was used to quantify cellular RNA. The primers used for qRT-PCR were as follows:

miR-25 (forward): 5'-CAT TGC ACT TGT CTC GGT CTG A-3′
miR-106b (forward): 5′-TAA AGT GCT GAC AGT GCA GAT-3′
miR-93 (forward): 5'-CAA AGT GCT GTT CGT GCA GGT AG-3′
miR-25, 106b, 93 (reverse): PerfeCTa universal reverse primer (Quanta).
βMHC (forward): 5'-CCC AAG GAA AAG AAG CAC GTC-3'
βMHC (reverse): 5′-AGG TCA GCT GGA TAG CGA CAT C-3'.
ANF (forward): 5'-CGA GCA GCG GAT TGA ACT GT-3'
ANF (reverse): 5′-TTG TGG TGA AGC CAC TCC TG-3'
BNP (forward): 5'-CTC CTA CTA CGA GCT GAA CCA G-3'
BNP (reverse): 5'-CCA GAA AGC TCA AAC TTG ACA GGC-3'
TGF-β1 (forward): 5'-CAA CAA TTC CTG GCG TTA CCT TGG-3'
TGF-β1 (reverse): 5′-GAA AGC CCT GTA TTC CGT CTC CTT-3'
Collagen type I, alpha 1 (forward): 5'-GCC AAG AAG ACA TCC CTG AAG-3'
Collagen type I, alpha 1 (reverse): 5′-TGT GGC AGA TAC AGA TCA AGC-3′
18s (forward): 5′-TAA CGA ACG AGA CTC TGG CAT-3′
18s (reverse): 5'-CGG ACA TCT AAG GGC ATC ACAG-3′

5.2. Chromatin immunoprecipitation

Chromatin was isolated from the right ventricle and the interventricular septum (50 mg) with the Imprint Chromatin Immunoprecipitation Kit (CHP1, Sigma) and ChIP DNA Clean & Concentrator Kit (D5201, Zymo Research) following the manufacturer's instructions. The immunoprecipitated chromatin, input, and IgG-bound chromatin were analyzed by qRT-PCR using the SYBR Green-based detection for the *MCM7* promoter or TaqMan-based detection for the *Six1* core promoter. The antibodies and sequences of probes used for qRT-PCR on immunoprecipitated chromatin were as follows:

H3K27me3: (07-449, Millipore, 1:50).

Suz12: (39,357, Active Motif, 1:50)

AcH3: (9677, Cell Signaling, 1:50)

Pol II: (R1530, Sigma, 1:50).

Six1: (12,891, Cell Signaling, 1:100)

MCM7 promoter forward primer: 5'-GGC CGT TCT GGA GAG TAG-3'

MCM7 promoter reverse primer: 5'-GCG CCG GGT TTC CCG CGG-3'

Six1 core promoter forward primer: 5'-CGA GGT TCG ACT GGT CTC TTC-3'

Six1 core promoter reverse primer: 5'-GCG CGG CTG CTC CTA A-3'

Six1 core promoter reporter sequence: 5'-CCC CTC CCT AGC CTT G-3′.

5.3. Bisulfite genomic sequencing

Methylation status of the *Six1* promoter in heart tissue samples obtained from mice with TAC-induced HF (TAC) and sham-operated mice (Sham) was assessed by bisulfite genomic sequencing. *Xho*I or *Eco*RI digested genomic DNA (5 μg) from these tissues was subjected to sodium bisulfite modification, and the *Six1* promoter was amplified as previously described [22]. The amplified product was subcloned into the pCR2.1 vector by TA cloning (Invitrogen) and sequenced via automated sequencing. Primer sequences for *Six1* promoter region amplification were as follows:

sense strand (−655 bp from TSS): 5′-GGG AAA AGT TAA GAT TGT AAG AGA TAG G-3′

antisense strand (−3 bp from TSS): 5′-AAT AAA CAA AAC TAA AAA AAC AAA AAA C-3′

sense strand (−813 bp from TSS): 5′-TTT TAT TTT TAG GAA TTA AAT TTG GAA GA-3′

antisense strand (+118 bp from TSS): 5′-AAA TTC CCT CCT TAC TAC AAA ACT TC-3′.

5.4. Statistical analysis

Data are expressed as mean ± s.e.m. as indicated. All data were analyzed using the Student's *t*-test for comparison of two groups and One-way ANOVA Bonferroni test for three groups. Survival testing was performed with the Kaplan–Meier analysis. To assess correlation coefficients, Spearman or Pearson correlation was used, and individual relative expression of genes (miR-25, *Six1*, *SERCA2a*, and *EED*) that were normalized by 18S RNA expression was plotted. For all in vivo experiments, the groups were randomly allocated and examined under blind test conditions. Statistical outliers were not automatically excluded; only technical failures or sudden death were excluded from the datasets. Differences were considered statistically significant when the p-value was < 0.05.

Supplementary data to this article can be found online at https://doi.org/10.1016/j.yjmcc.2019.01.017.

Author contributions

J.G.O., W.J.P., and D.J. designed the research, performed the experiments, analyzed the data, and wrote the paper. S.P.J., M.L., S.H.L., T.L., E.J., and J.Y. contributed in performing experiments and review the manuscript. C.K. and H.K. served as scientific advisors, R.J.H., W.J.P., and D.J. revised the data and performed a final revision of data.

Acknowledgements

We specially thank to Ms. Okkil Kim and Dr. Lifan Lian for the generation of adeno-associated viruses (AAV) and adenoviruses (Ad). This work is supported by NIHR01 HL117505, HL119046, HL129814, HL128072, HL131404, HL135093, P50 HL112324, and a Transatlantic Foundation Leducq grant. Dr. Park was supported by a Basic Science Research Program (2017R1A2B4007340) and a Bio & Medical Technology Development Program (2015M3A9E6028951) from NRF of Korea. Drs. Park and Kook were supported by a Basic Research Laboratory Program (2016R1A4A1009895) from NRF of Korea. Dr. Jeong was supported by the Assistant Secretary of Defense for Health Affairs endorsed by the Department of Defense, through the FY17, DMDRP, Career Development Award Program under Award No. W81XWH-18-1-0322. J.G.O was supported by AHA17POST33410877.

Conflict of interest

Dr. Hajjar has ownership interest in Nanocor and Sumocor. Drs. Hajjar and Park have co-ownership interest in Bethphagen. The other authors have declared that no conflict of interest exists.

References

[1] E.J. Benjamin, S.S. Virani, C.W. Callaway, A.M. Chamberlain, A.R. Chang, S. Cheng, S.E. Chiuve, M. Cushman, F.N. Delling, R. Deo, et al., Heart disease and stroke Statistics-2018 update: a report from the American Heart Association, Circulation 137 (12) (2018) e67–e492.

[2] M. Meyer, W. Schillinger, B. Pieske, C. Holubarsch, C. Heilmann, H. Posival, G. Kuwajima, K. Mikoshiba, H. Just, G. Hasenfuss, et al., Alterations of sarcoplasmic reticulum proteins in failing human dilated cardiomyopathy, Circulation 92 (4) (1995) 778–784.

[3] Y. Kawase, H.Q. Ly, F. Prunier, D. Lebeche, Y. Shi, H. Jin, L. Hadri, R. Yoneyama, K. Hoshino, Y. Takewa, et al., Reversal of cardiac dysfunction after long-term expression of SERCA2a by gene transfer in a pre-clinical model of heart failure, J. Am. Coll. Cardiol. 51 (11) (2008) 1112–1119.

[4] C. Wahlquist, D. Jeong, A. Rojas-Munoz, C. Kho, A. Lee, S. Mitsuyama, A. van Mil, W.J. Park, J.P. Sluijter, P.A. Doevendans, et al., Inhibition of miR-25 improves cardiac contractility in the failing heart, Nature 508 (7497) (2014) 531–535.

[5] J.T. Mendell, miRiad roles for the miR-17-92 cluster in development and disease, Cell 133 (2) (2008) 217–222.

[6] A.L. Smith, R. Iwanaga, D.J. Drasin, D.S. Micalizzi, R.L. Vartuli, A.C. Tan, H.L. Ford, The miR-106b-25 cluster targets Smad7, activates TGF-beta signaling, and induces EMT and tumor initiating cell characteristics downstream of Six1 in human breast cancer, Oncogene 31 (50) (2012) 5162–5171.

[7] P. Delgado-Olguin, Y. Huang, X. Li, D. Christodoulou, C.E. Seidman, J.G. Seidman, A. Tarakhovsky, B.G. Bruneau, Epigenetic repression of cardiac progenitor gene expression by Ezh2 is required for postnatal cardiac homeostasis, Nat. Genet. 44 (3) (2012) 343–347.

[8] D. Jeong, J. Yoo, P. Lee, S.V. Kepreotis, A. Lee, C. Wahlquist, B.D. Brown, C. Kho, M. Mercola, R.J. Hajjar, miR-25 tough decoy enhances cardiac function in heart failure, Mol. Ther. 26 (3) (2018) 718–729.

[9] J. Aguero, K. Ishikawa, L. Hadri, C.G. Santos-Gallego, K.M. Fish, E. Kohlbrenner, N. Hammoudi, C. Kho, A. Lee, B. Ibanez, et al., Intratracheal gene delivery of SERCA2a ameliorates chronic post-capillary pulmonary hypertension: a large animal model, J. Am. Coll. Cardiol. 67 (17) (2016) 2032–2046.

[10] B. Greenberg, A. Yaroshinsky, K.M. Zsebo, J. Butler, G.M. Felker, A.A. Voors, J.J. Rudy, K. Wagner, R.J. Hajjar, Design of a phase 2b trial of intracoronary administration of AAV1/SERCA2a in patients with advanced heart failure: the CUPID 2 trial (calcium up-regulation by percutaneous administration of gene therapy in cardiac disease phase 2b), JACC Heart Fail. 2 (1) (2014) 84–92.

[11] R.J. Hajjar, K. Zsebo, L. Deckelbaum, C. Thompson, J. Rudy, A. Yaroshinsky, H. Ly, Y. Kawase, K. Wagner, K. Borow, et al., Design of a phase 1/2 trial of intracoronary administration of AAV1/SERCA2a in patients with heart failure, J. Card. Fail. 14 (5) (2008) 355–367.

[12] J.S. Hulot, J.E. Salem, A. Redheuil, J.P. Collet, S. Varnous, P. Jourdain, D. Logeart, E. Gandjbakhch, C. Bernard, S.N. Hatem, et al., Effect of intracoronary administration of AAV1/SERCA2a on ventricular remodelling in patients with advanced systolic heart failure: results from the AGENT-HF randomized phase 2 trial, Eur. J. Heart Fail. 19 (11) (2017) 1534–1541.

[13] M.G. Katz, E. Brandon-Warner, A.S. Fargnoli, R.D. Williams, A.P. Kendle, R.J. Hajjar, L.W. Schrum, C.R. Bridges, Mitigation of myocardial fibrosis by molecular cardiac surgery-mediated gene overexpression, J. Thorac. Cardiovasc. Surg.

151 (4) (2016) 1191–1200 (e3).
[14] B. Strauss, Y. Sassi, C. Bueno-Beti, Z. Ilkan, N. Raad, M. Cacheux, M. Bisserier, I.C. Turnbull, E. Kohlbrenner, R.J. Hajjar, et al., Intra-tracheal gene delivery of aerosolized SERCA2a to the lung suppresses ventricular arrhythmias in a model of pulmonary arterial hypertension, J. Mol. Cell. Cardiol. 127 (2018) 20–30.
[15] S. Watanabe, K. Ishikawa, M. Plataki, O. Bikou, E. Kohlbrenner, J. Aguero, L. Hadri, I. Zarragoikoetxea, K. Fish, J.A. Leopold, et al., Safety and long-term efficacy of AAV1.SERCA2a using nebulizer delivery in a pig model of pulmonary hypertension, Pulm. Circ. 8 (4) (2018) 2045894018799738.
[16] K. Zsebo, A. Yaroshinsky, J.J. Rudy, K. Wagner, B. Greenberg, M. Jessup, R.J. Hajjar, Long-term effects of AAV1/SERCA2a gene transfer in patients with severe heart failure: analysis of recurrent cardiovascular events and mortality, Circ. Res. 114 (1) (2014) 101–108.
[17] P.A. Bidwell, G.S. Liu, N. Nagarajan, C.K. Lam, K. Haghighi, G. Gardner, W.F. Cai, W. Zhao, L. Mugge, E. Vafiadaki, et al., HAX-1 regulates SERCA2a oxidation and degradation, J. Mol. Cell. Cardiol. 114 (2018) 220–233.
[18] C. Kho, A. Lee, D. Jeong, J.G. Oh, A.H. Chaanine, E. Kizana, W.J. Park, R.J. Hajjar, SUMO1-dependent modulation of SERCA2a in heart failure, Nature 477 (7366) (2011) 601–605.
[19] J.G. Oh, S. Watanabe, A. Lee, P.A. Gorski, P. Lee, D. Jeong, L. Liang, Y. Liang, A. Baccarini, S. Sahoo, et al., miR-146a suppresses SUMO1 expression and induces cardiac dysfunction in maladaptive hypertrophy, Circ. Res. 123 (6) (2018) 673–685.
[20] C. Quan, M. Li, Q. Du, Q. Chen, H. Wang, D.G. Campbell, L. Fang, B. Xue, C. MacKintosh, X. Gao, et al., SPEG controls calcium re-uptake into the sarcoplasmic reticulum through regulating SERCA2a by its second kinase-domain, Circ. Res. (2018) Ahead of Print.
[21] D. Zhao, X. Li, H. Liang, N. Zheng, Z. Pan, Y. Zhou, X. Liu, M. Qian, B. Xu, Y. Zhang, et al., SNX17 produces anti-arrhythmic effects by preserving functional SERCA2a protein in myocardial infarction, Int. J. Cardiol. 272 (2018) 298–305.
[22] R. Milani, Two new eye-shape mutant alleles in Drosophila melanogaster, DIS 14 (1941).
[23] N.M. Bonini, W.M. Leiserson, S. Benzer, The eyes absent gene: genetic control of cell survival and differentiation in the developing Drosophila eye, Cell 72 (3) (1993) 379–395.
[24] S. Abdelhak, V. Kalatzis, R. Heilig, S. Compain, D. Samson, C. Vincent, D. Weil, C. Cruaud, I. Sahly, M. Leibovici, et al., A human homologue of the Drosophila eyes absent gene underlies branchio-Oto-renal (BOR) syndrome and identifies a novel gene family, Nat. Genet. 15 (2) (1997) 157–164.
[25] B.N. Cheyette, P.J. Green, K. Martin, H. Garren, V. Hartenstein, S.L. Zipursky, The Drosophila sine oculis locus encodes a homeodomain-containing protein required for the development of the entire visual system, Neuron 12 (5) (1994) 977–996.
[26] C. Dozier, H. Kagoshima, G. Niklaus, G. Cassata, T.R. Burglin, The Caenorhabditis elegans six/sine oculis class homeobox gene ceh-32 is required for head morphogenesis, Dev. Biol. 236 (2) (2001) 289–303.
[27] D. Hoshiyama, N. Iwabe, T. Miyata, Evolution of the gene families forming the Pax/six regulatory network: isolation of genes from primitive animals and molecular phylogenetic analyses, FEBS Lett. 581 (8) (2007) 1639–1643.
[28] M. Jin, S. Aibar, Z. Ge, R. Chen, S. Aerts, G. Mardon, Identification of novel direct targets of Drosophila sine oculis and eyes absent by integration of genome-wide data sets, Dev. Biol. 415 (1) (2016) 157–167.
[29] K. Kawakami, S. Sato, H. Ozaki, K. Ikeda, Six family genes–structure and function as transcription factors and their roles in development, BioEssays 22 (7) (2000) 616–626.
[30] I. Sahly, P. Andermann, C. Petit, The zebrafish eya1 gene and its expression pattern during embryogenesis, Dev. Genes Evol. 209 (7) (1999) 399–410.
[31] H.C. Seo, J. Curtiss, M. Mlodzik, A. Fjose, Six class homeobox genes in drosophila belong to three distinct families and are involved in head development, Mech. Dev. 83 (1–2) (1999) 127–139.
[32] M.A. Serikaku, J.E. O'Tousa, Sine oculis is a homeobox gene required for Drosophila visual system development, Genetics 138 (4) (1994) 1137–1150.
[33] P.X. Xu, I. Woo, H. Her, D.R. Beier, R.L. Maas, Mouse Eya homologues of the Drosophila eyes absent gene require Pax6 for expression in lens and nasal placode, Development 124 (1) (1997) 219–231.
[34] A. He, Q. Ma, J. Cao, A. von Gise, P. Zhou, H. Xie, B. Zhang, M. Hsing, D.C. Christodoulou, P. Cahan, et al., Polycomb repressive complex 2 regulates normal development of the mouse heart, Circ. Res. 110 (3) (2012) 406–415.
[35] E. Vire, C. Brenner, R. Deplus, L. Blanchon, M. Fraga, C. Didelot, L. Morey, A. Van Eynde, D. Bernard, J.M. Vanderwinden, et al., The Polycomb group protein EZH2 directly controls DNA methylation, Nature 439 (7078) (2006) 871–874.
[36] S. Suzuki, A. Adachi, A. Hiraiwa, M. Ohashi, M. Ishibashi, T. Kiyono, Cloning and characterization of human MCM7 promoter, Gene 216 (1) (1998) 85–91.